Application of Binocular Vision Algorithm Based on Measurement and Control Technology in Robot Measurement and Positioning

Hongwei Duan
Department of Mechatronics, Shanxi Polytechnic College, Taiyuan 030006, China
E-mail: duanhongwei6@163.com

Keywords: binocular stereo vision, target matching algorithm, spatial three-dimensional coordinates, visual guidance, robot measurement and positioning

Received: June 13, 2024

Due to the efficient application of computer vision technology in automation industry, the research on robot measurement and positioning combined with binocular vision algorithms and visual guidance systems has become more advanced and complex. This paper uses binocular vision information to construct spatial three-dimensional coordinates, and then issues execution commands to the robot, so that the geometric modeling of binocular stereo vision can meet the requirements of accurate measurement and positioning of test targets. The target matching algorithm for binocular stereo vision is analyzed and the most suitable block matching algorithm for machine perfusion is determined. It belongs to the local matching algorithm and has a calculation speed of 93 ms. The parameters and spatial coordinate positioning measurement results of the left and right cameras were tested, and the results demonstrated that the pixel focal lengths of the left camera were 8.10172 mm and 8.10407 mm, respectively. The pixel focal lengths of the right camera were 8.10140 mm and 8.10365 mm. The maximum projection error of the left and right cameras was 0.075 pixels. The maximum and average error results of the 29 honeycomb structural components tested subsequently were 1.16 mm, 0.63 mm, and 1.83 mm, 0.81 mm on the horizontal and vertical axes, respectively. The maximum error value in rotation angle was 3.56°, and the average value was 1.37°. The final results indicated that the error remained within approximately 2 mm and 4°. The experimental data demonstrate that the algorithm system has precise requirements for robot measurement and positioning, and provides a theoretical basis and technical reference for robot measurement and positioning.

Povzetek: Opisan je algoritem binokularnega vida za merjenje in pozicioniranje robotov. Prispevek z uporabo binokularne stereo vizije in algoritma za ujemanje ciljev izboljšuje prostorske meritve in pozicioniranje robotov, kar omogoča bolj učinkovito avtomatizacijo industrijskih procesov.

1 Introduction

The research and application of industrial robots (IROs) is a major hotspot in industrial automation at present and in the future. With the fast growth of computer science, computer vision technology has become more widely used in the industrial field and provides scientific basis for the development of intelligent IRO. The robot visual guidance system (RVGS) is divided into visual guidance of position and image, and the image acquisition information technology of left and right cameras is used for binocular stereo vision (BSV) matching in industrial manufacturing [1]. Binocular vision represents a refinement of understanding and adapting to the environment. Stereo vision, in particular, is the most advanced function of binocular vision. It enables the establishment of stereo cognition of object shape, azimuth, distance, and spatial range. This, in turn, facilitates creative breakthroughs in the human labor process [2]. In modern society, the use of sports technology, medical instruments, and technological instruments all utilize the principle of stereoscopic vision, which provides effective assistance for engineering production and other aspects. In particular, the trajectory of sports balls has a considerable impact on real-time tracking, thereby facilitating the enhancement of training for sporting events. In regard to positioning and obstacle avoidance, stereo vision offers the benefits of robot automation and intelligence through the ability to navigate cleanly and avoid obstacles on a given path. Additionally, it enables robots to accurately measure and locate objects [3, 4]. In recent years, many scholars have conducted many discussions on robot measurement positioning, binocular vision algorithms, etc., providing theoretical basis and technical support for the improvement of binocular vision algorithms. Based on this, the paper deeply discusses the Geometric modeling of BSV, seeks its optimal target matching algorithm, and constructs the vision guidance system of the IRO. It is intended to provide scientific references for the improvement of binocular vision algorithm applications and the precise measurement and positioning technology of IRO.

The content has four parts. The first part elaborates on the research and application of current binocular vision

algorithms. The second part describes the Geometric modeling framework of BSV, and explains the basic technology and application of BSV. The third part is to conduct experimental analysis on the target matching algorithm of BSV to obtain the most suitable target matching algorithm. The final part is a narrative summary of the entire study.

2 Related works

The robot measurement and positioning technology mainly lies in the research and application of computer vision technology. At present, it is widely used in RVGSs, including position and image-based visual guidance. In recent years, many scholars have conducted extensive analysis on algorithms and technologies related to robot measurement and positioning. Zhi et al. proposed using an infrared binocular vision system to establish a badminton trajectory dataset for badminton robots. They designed filtering algorithms to construct trajectory prediction models, thereby obtaining real-time and efficient motion trajectories of flying objects [5]. The camera calibration based on a binocular vision system ensured the real-time tracking of the vision system and proved the generalizability of robot measurement and positioning in motion projects. For the application of obstacle avoidance robot, Zhang proposed a binocular vision navigation method to calibrate the camera for the visual navigation problem of the marine garbage cleaning robot. It used dynamic obstacle avoidance algorithms to plan the mobile route, thereby achieving efficient robot positioning and path planning [6]. Regarding the application of autonomous navigation obstacle avoidance robots, Ren H proposed using computer vision theory to design an intelligent robot path avoidance system. The binocular vision ranging experiment has demonstrated the excellent performance of the intelligent robot in obstacle avoidance [7]. Wang et al. proposed a visual binocular obstacle detection method to obtain positional parameters in response to the problem of obstacles in the field, and summarized methods for detecting obstacles in the field [8]. Robots often use binocular vision algorithms to accurately obtain information in positioning technologies such as clean navigation and path obstacle avoidance, thereby ensuring the intelligent working mode of the robot. Wei H et al. proposed using line segments and edges as matching algorithms to identify 2D and 3D corresponding relationships for high-precision robot applications. Combining deep learning algorithms, it provided technical support for binocular visual guidance of IRO to demonstrate the good application of robotic arms [9]. Zhang proposed using image segmentation algorithms for object extraction in the visual system to address the issue of harvesting robots, thereby establishing a color space reference table for real-time processing of image information by the robot [10]. The application of robots in grasping or picking objects also used binocular vision systems to assist in accurate measurement and positioning of objects. For image processing of instrument robots, Han J proposed using BSV technology to obtain 3D image information of characters and solve the problem of robot recognition and positioning. This idea has achieved research results in industrial manufacturing, automation and other fields [11]. Wen et al. conducted single-arm grasping experiments using binocular vision algorithms combined with dual-arm collaborative robots and visual-guided image processing on issues related to intelligent manufacturing robot engineering. Therefore, the accuracy and stability of robot actions could be improved [12]. Li et al. believed that the core of robotic arm sorting lies in speed and accuracy, and proposed using binocular cameras and deep learning algorithms to perform image processing and grasping experiments. This system had high speed and accuracy [13]. In terms of scientific instruments, robots use binocular vision algorithms to process images and improve the accuracy of machine operation. In other aspects of production and daily life, Jian et al. proposed the use of mean filtering method combined with binocular vision cameras to accurately guide robot wiring regarding the identification and positioning of main transmission lines [14]. Gao et al. proposed using transformation algorithms to achieve image pre-matching and improve the pre-matching results in response to the issues of detection speed and accuracy of parallel robots. The high-precision detection of parallel robots based on binocular vision has been proven [15]. Wang et al. proposed a fast detection method based on binocular vision and combined with block matching algorithm to obtain pipeline information to achieve real-time detection of pipeline inner diameter in response to the problem of pipeline automatic detection [16]. Robot measurement and positioning technology has been promoted in various fields, but it still requires extensive research and application in multiple fields and at a deeper level.

In summary, industry scholars have established many binocular vision systems and systematic methods for robot measurement and positioning. However, there is a lack of measurement and recognition of the external contours of dense and complex structural components, as well as robot positioning algorithms, which can easily affect the accuracy of part manufacturing. In the system operation of IROs in grasping and sorting, the processing of visual images cannot directly meet the requirements of industrial operations. This is due to the limited utilization of basic and complex components by manufacturing robots in target extraction applications. Moreover, there is a lack of close connection between stereo binocular vision technology and the operation of robot systems. Therefore, more advanced visual technology is needed in the production of basic parts to achieve complex contour recognition and measurement positioning problems. Therefore, this study utilizes a binocular vision algorithm based on measurement and control technology for contour recognition of complex honeycomb components. By utilizing stereo matching algorithm to achieve data detection and imaging of components, real-time

measurement and precise positioning can be achieved in infusion operations, proving its high advantages in robot measurement and positioning.

The Summary Table of Relevant Literature is in table 1.

Table 1: Summary table of relevant literature

Reference number	Research methods	Research results
Zhi et al [5]	Establish a badminton trajectory dataset using an infrared binocular vision system, and then design a filtering algorithm to construct a trajectory prediction model.	Obtain real-time and efficient motion trajectories of flying objects.
Zhang [6]	Calibrate the camera using binocular vision navigation method and plan the movement route using dynamic obstacle avoidance algorithm.	Realize efficient positioning and path planning of marine garbage cleaning robots.
Ren [7]	Design an intelligent robot path avoidance system using computer vision theory.	Proved the good effect of intelligent robot obstacle avoidance.
Wang et al [8]	Obstacle detection method based on visual binocular to obtain position parameters.	Summarize effective detection methods for obstacles in farmland and wilderness.
Wei et al [9]	Using line segments and edges as matching algorithms to find the correspondence between 2D and 3D, and combining deep learning algorithms to design binocular vision guidance technology for industrial robots.	Proving the good application and high-precision measurement of robotic arms.
Zhang [10]	Use image segmentation algorithms for object extraction in visual systems.	A color space reference table has been established for the robot to process image information in real-time.
Han [11]	Using binocular stereo vision technology to obtain three-dimensional image information of characters.	Obtained research results in robot recognition and positioning in industrial manufacturing and automation fields.
Wen et al [12]	Constructing a dual arm collaborative robot using binocular vision algorithms and visual guided image processing.	Through single arm grasping experiments, the accuracy and stability of robot movements can be improved.
Li et al [13]	Utilize binocular cameras and deep learning algorithms to perform image processing and capture experiments.	Proving the high speed and precision of the robotic arm sorting system.
Jian et al [14]	Design robot localization using mean filtering method and binocular vision camera.	Effectively achieving the precision of robot wiring.
Gao et al [15]	Use transformation algorithms to achieve image pre matching and improve pre matching results.	Proved the high accuracy of parallel robot detection based on binocular vision.
Wang et al [16]	Propose a fast detection method based on binocular vision and combine it with block matching algorithm to obtain pipeline information.	Real time detection and automation performance of pipeline inner diameter have been achieved.

3 Model construction and matching algorithm design of BSV

In modern society, the role of robot measurement and positioning in production and life is becoming increasingly important. The research on the technology of using stereo vision principles to construct binocular stereo models for positioning and matching test targets has provided effective assistance.

3.1 Geometric modeling of BSV

This paper utilizes binocular visual information to construct three-dimensional structures in real space and extract three-dimensional coordinates, thereby guiding robots to perform related actions. The commonly used coordinate systems in BSV include world, image, and

camera coordinate systems (CCS). The world coordinate system (WCS) is utilized to elaborate the related point of the camera in the spatial environment, and its origin and coordinate axis can be located in any right-hand system of spatial coordinates. The image coordinate system (ICS) usually has two forms of representation, namely the x and y axis coordinate system in the units of length and the u and v axis in pixels. The origin of the x and y is the midpoint of the plane in the u and v coordinate systems, and the spatial size of each pixel on the x and y axes is represented as kx and ky, respectively. The connection between two planar coordinate systems is equation (1).

$$\begin{cases} u = \dfrac{x}{kx} + u_1 \\ v = \dfrac{y}{ky} + v_1 \end{cases} \tag{1}$$

In equation (1), u_1 is the midpoint of the u axis and the origin of the x axis, while v_1 is the midpoint of the v and the origin of the y. The CCS is a coordinate system that changes based on the spatial position of the camera. Its origin is at the focal point of the camera lens, and the two coordinate axes X and Y are parallel to the x and y axes of the ICS. Modern camera imaging is based on a small aperture imaging model, where the image information received by the camera is inverted, resulting in a three-dimensional image. According to the mapping relationship, the position of any point $P(X_d, Y_d, Z_d)$ in the CCS in the ICS (x, y) is equation (2).

$$\begin{cases} x = \dfrac{fX_d}{Z} \\ y = \dfrac{fY_d}{Z} \end{cases} \tag{2}$$

In equation (2), f is the distance from the focal point of the lens in the small hole imaging model to the received image, i.e., the focal length. The manifestation of the projective relationship is a matrix, as shown in equation (3).

$$Z_d \begin{bmatrix} x \\ y \\ 1 \end{bmatrix} = \begin{bmatrix} f & 0 & 0 & 0 \\ 0 & f & 0 & 0 \\ 0 & 0 & 1 & 0 \end{bmatrix} \begin{bmatrix} X_d \\ Y_d \\ Z_d \\ 1 \end{bmatrix} \tag{3}$$

In equation (3), x and y are the coordinate axes of the ICS. The imaging results of the camera are only connected with the internal structure of the camera, while the standing posture in the external WCS determines the imaging results of the camera, which together form the projection matrix relationship of the camera.

The three-dimensional coordinates of BSV are calculated using the principle of parallax and triangulation. When the BSV positions of the two cameras are in the Standard state, that is, height $h = y_a = y_b$ and parallax $e = x_a = x_b$. According to the Similar triangle's theorem, the equation (4) is obtained.

$$\begin{cases} \dfrac{x_a}{f} = \dfrac{X_d}{Z_d} \\ \dfrac{x_b}{f} = \dfrac{X_d - L}{Z_d} \\ \dfrac{h}{f} = \dfrac{Y_d}{Z_d} \end{cases} \tag{4}$$

In equation (4), h is the vertical height of the camera, and f is the focal length of the aperture imaging model. Then, based on the internal and external parameters of the camera and the position of the target point on the left and right cameras, the three-dimensional coordinate position of the point is calculated, as shown in equation (5).

$$\begin{cases} X_d = \dfrac{L * x_a}{e} \\ Y_d = \dfrac{L * h}{e} \\ Z_a = \dfrac{L * f}{e} \end{cases} \tag{5}$$

In equation (5), e represents the parallax between two cameras at standard positions, and L represents the horizontal distance between the two cameras. When two cameras do not meet the standard position, additional parameters need to be added. Then the WCS is overlapped with the left camera and set to $O_a - X_a Y_a Z_a$. Its origin is still in the focal position, and the focal length is set to f_a. The ICS of the left camera is changed to $o_a - x_a y_a z_a$. At the same time, the coordinate system of the right camera is $O_b - X_b Y_b Z_b$. If the origin remains unchanged, the focal length is set to f_b, and the ICS becomes $o_b - x_b y_b z_b$. At this point, the matrix relationship of the camera projection is shown in equations (6) and (7).

$$Z_a \begin{bmatrix} x_a \\ y_a \\ z_a \end{bmatrix} = \begin{bmatrix} f_a & 0 & 0 & 0 \\ 0 & f_a & 0 & 0 \\ 0 & 0 & 1 & 0 \end{bmatrix} \begin{bmatrix} X_a \\ Y_a \\ Z_a \\ 1 \end{bmatrix} \tag{6}$$

f_a in equation (6) is the focal length of the left camera.

$$Z_b\begin{bmatrix} x_b \\ y_b \\ 1 \end{bmatrix}=\begin{bmatrix} f_b & 0 & 0 & 0 \\ 0 & f_b & 0 & 0 \\ 0 & 0 & 1 & 0 \end{bmatrix}\begin{bmatrix} X_b \\ Y_b \\ Z_b \\ 1 \end{bmatrix} \quad (7)$$

In equation (7), f_b is the focal length of the right camera. Furthermore, a spatial transformation matrix S is taken to represent the positional relationship between the current left& right CCSs, as shown in equations (8) and (9).

$$\begin{bmatrix} X_b \\ Y_b \\ Z_b \end{bmatrix}=S\begin{bmatrix} X \\ Y \\ Z \\ 1 \end{bmatrix}=\begin{bmatrix} N_{11} & N_{12} & N_{13} & G_x \\ N_{21} & N_{22} & N_{23} & G_y \\ N_{31} & N_{32} & N_{33} & G_z \end{bmatrix}\begin{bmatrix} X \\ Y \\ Z \\ 1 \end{bmatrix} \quad (8)$$

In equation (8), N and G represent the Rotation matrix and translation vector from the left CCS to the right CCS, respectively.

$$S=\begin{bmatrix} N & G \end{bmatrix} \quad (9)$$

In equation (9), S is the spatial transformation matrix. Then the equations (6) and (7) are substituted into equation (8) to obtain the projection points of point P in the spatial coordinate system in the left and right ICSs. The matrix relationship between the two projection points is shown in equation (10).

$$\begin{bmatrix} x_b \\ y_b \\ 1 \end{bmatrix}=\frac{1}{Z_b}\begin{bmatrix} f_bN_{11} & f_bN_{12} & f_bN_{13} & f_bG_x \\ f_bN_{12} & f_bN_{22} & f_bN_{23} & f_bG_y \\ N_{31} & N_{32} & N_{33} & G_z \end{bmatrix}\begin{bmatrix} \frac{Zx_a}{f_a} \\ \frac{Zy_a}{f_a} \\ Z \\ 1 \end{bmatrix} \quad (10)$$

Equation (10) represents the projection points P_a and P_b of space point P in the left&right ICSs. Finally, the three-dimensional coordinate position of space point P is calculated, as shown in equation (11).

$$\begin{cases} X=\frac{Zx_a}{f_a} \\ Y=\frac{Zy_a}{f_a} \\ Z=\frac{f_a\left(f_bG_x-x_bG_z\right)}{x_b\left(N_{31}x_a+N_{32}y_a+N_{33}f_a\right)-f_b\left(N_{11}x_a+N_{12}y_a+N_{13}f_a\right)} \end{cases} \quad (11)$$

Given a point in space located at two coordinate points in the left and right ICS, as well as the focal length of the left and right cameras and the positional relationship between the cameras, the three-dimensional coordinates of that point can be calculated.

3.2 Target matching algorithm for BSV

In the left and right images, the corresponding feature relationships are found, which correspond to the projected light points of a certain point in space in the left and right images. The resulting disparity map is a stereo matching of BSV. Stereo matching is a key and difficult point in BSV localization. When a 3D scene is projected onto a 2D image, the imaging results of the same object may vary from different perspectives. Moreover, changes in external factors can affect the grayscale values of image pixels to obtain accurate stereo matching results. Currently, various binocular stereo matching algorithms have been proposed for application in different environments. Zhou et al. proposed a 3D reconstruction method grounded on binocular vision to locate cutting points on retinal blood vessels in response to issues related to robot-assisted ophthalmic surgery. They used algorithms for stereo matching to reconstruct retinal vascular images, proving that this method can accurately locate cutting points and meet the needs of medical ophthalmic surgery [17]. Hu et al. proposed a visual detection method built on deep learning and utilized visual measurement and control technology to operate the robot for repairing broken strands in input circuit. This proved the feasibility of robot structure design and the effectiveness of visual control algorithms [18].

According to different constraint methods, stereo matching algorithms are segmented into local and global stereo matching algorithms. However, in the current research progress, mature stereo matching algorithms for binocular vision systems mainly include block matching (BM), semi-global block matching (SGBM), and graph cut (GC) algorithms. BM is mainly divided into four steps, namely line alignment, pre-filtering, matching search, and re-filtering. The search for the optimal matching point requires certain matching conditions, as shown in equation (12).

$$T(x,y,w)=\sum_{(x,y)\in W}\left|H_a(x,y)-H_b(x+w,y)\right| \quad (12)$$

In equation (12), w is the displacement of the window, W is the window size, and H is the grayscale value of the pixels in the matching window. The smaller the value of the matching condition, the higher the matching degree. In the BM algorithm, the important factors that affect calculation speed and matching results are sum of absolute difference (SAD), window size, minimum disparity, number of disparity, and uniqueness ratio (UR). The larger the window size, the more information it contains and the higher the matching accuracy, but the computational time used will continue to increase. The minimum disparity determines the initial position of the matching search. The amount of disparity determines the number of pixels to be searched during the matching point search process. The two jointly determine the search range for matching points corresponding to the left image in the right image, as shown in Figure 1.

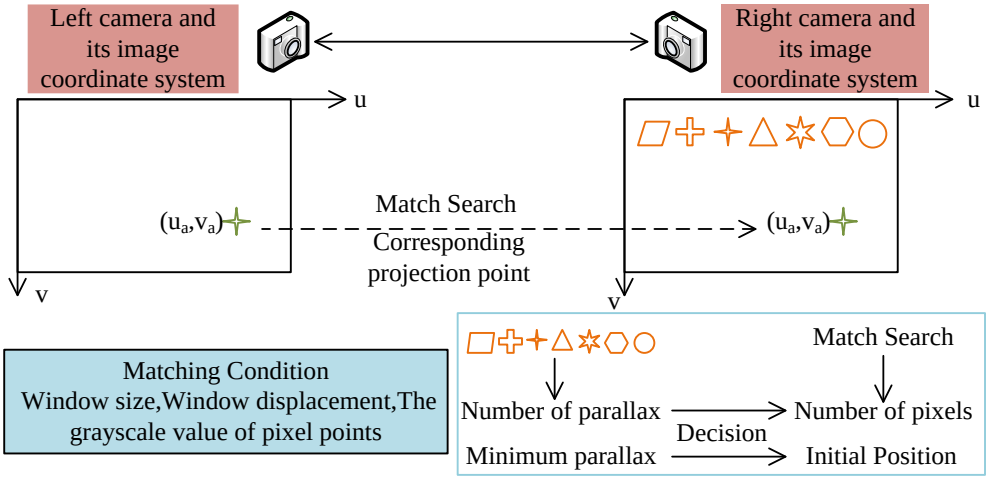

Figure 1: Schematic diagram of BM algorithm

In Figure 1, when a point in the left ICS corresponds to the search range of matching points in the right ICS, it represents all pixel points that pass through the process of moving the number of parallaxes left from the minimum parallax on the same polar line. The value of the number of parallaxes determines the search length, so its selection should be the minimum value. The method of selecting values needs to be combined with the minimum parallax, and substituted into the parallax formula, as shown in equation (13).

$$e=\frac{L*A}{2h*\tan\frac{\alpha}{2}} \quad (13)$$

In equation (13), L is the reference distance between the left and right cameras. A is the pixel in the base distance direction, and α is the camera angle. The general range of disparity is found and combined with the number of selected disparities and the minimum disparity. This range is included in the search scope. The percentage of disparity uniqueness is a functional function of matching, which aims to prevent the occurrence of incorrect matching, as expressed in equation (14).

$$T_{\text{Minimum}}\le\frac{1+UniquenessRatio}{100}T_{\text{Secondary Minimum}} \quad (14)$$

In equation (14), T_{Minimum} is the lowest matching condition and $T_{\text{Secondary Minimum}}$ is the second lowest matching condition. Only when this equation is met, the disparity value (DV) corresponding to the lowest matching condition is considered as the DV of the pixel, otherwise the DV of the pixel is 0. The larger the value of the uniqueness percentage of disparity, the lower the matching error rate, and usually the range of values is between 3 and 15. Another stereo matching algorithm, SGBM, belongs to the sem-global matching algorithm. Firstly, an energy function is constructed, then matching conditions are set based on multi-directional search range. Finally, the optimal values of the energy function and matching conditions are solved. The energy function is shown in equation (15).

$$E(D)=\sum_m\left(T(m,D_m)+\sum_{n\in N_m}P_1I\left[|D_m-D_n|=1\right]+\sum_{n\in N_m}P_2I\left[|D_m-D_n|>1\right]\right) \quad (15)$$

In equation (15), D is the parallax image, and $E(D)$ is the energy function of the parallax image. m and n are pixels in the image. N_m represents the eight

surrounding pixels centered on pixel m. $T(m, D_m)$ represents the matching condition when the depth value of pixel m is taken as D_m. P_1 and P_2 are penalty coefficients. $I[...]$ is a Boolean variable. At present, the visual guidance of IRO is widely used in the field of modern industrial manufacturing. The measurement and positioning of robots are based on the visual guidance system receiving image information and position information, and then processing the information to complete work instructions. The image processing system is the core of robot operation, which can improve work efficiency and enhance the intelligence level of IRO. Its excellent processing system is thanks to the development of computer vision. Computer vision is used for typical IRO vision guidance system, which usually has four main systems, as shown in Figure 2.

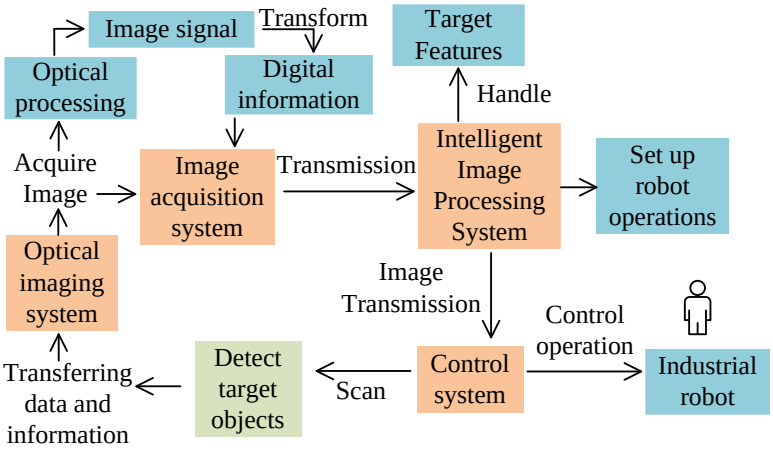

Figure 2: Structure of a typical industrial RVGS

In Figure 2, the main structures of the industrial RVGS include optical imaging, image acquisition, intelligent image processing, and control execution systems. A mature and complete IRO automatic positioning control cellular software system should have five main functions, including communication, data processing, human-machine interaction, scalability, and high-speed response. Due to the complex shape of honeycomb structural components, their imaging structure is unstable and easily affected by factors such as light and perspective, which can affect the visual detection of positioning robots. Therefore, after analyzing the key and difficult points of honeycomb structure features, a robot localization method based on BSV measurement for eye in hand visual detection system has been proposed. Figure 3 shows the structure of the robot control positioning software.

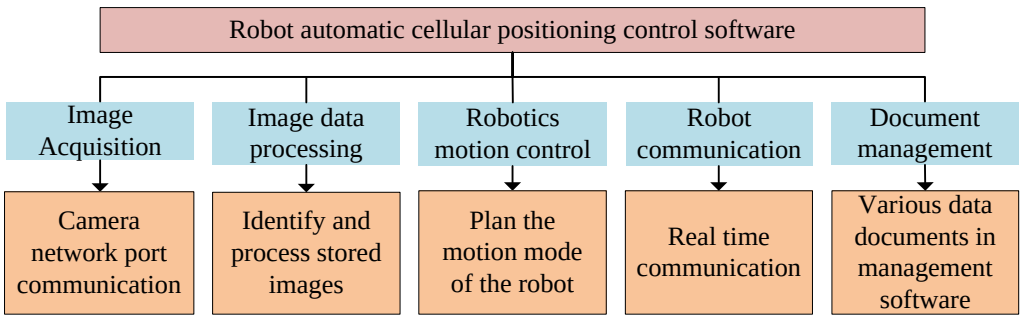

Figure 3: Framework of robot control positioning software

In Figure 3, the software control system based on the Microsoft foundation classes (MFC) framework not only needs to meet basic robot control operation requirements, but also needs to meet performance requirements such as data exchange, efficient data processing, status monitoring, and real-time feedback of results. The main functions of a complete IRO automatic cellular positioning system control software include: supporting communication between different hardware functions, converting data processing functions, real-time human-machine interaction function for feedback information, scalability function, and high-speed response function for command interaction. These functions not only reduce the workload and development costs of developers, but also greatly reduce the workload of workers in industrial manufacturing.

4 Analysis of robot measurement and positioning experiment

The maximum working radius of the six degree of freedom IRO selected for research is 2500mm, the maximum end load is 120kg, and the repeatability positioning accuracy is between -0.06mm and 0.06mm. The control system used is KR C4, and the teaching pendant is KUKA smart PAD, indicating that the robot's setup is simple and precise. A binocular camera is installed at the end of the IRO and connected between the infusion head and the infusion device. It uses extremely small infusion heads to detect honeycomb structures and collect internal information. Based on the mature application of stereo matching algorithms in binocular vision systems and the binocular calibration images of left and right cameras, experimental analysis is conducted on the measurement and positioning of honeycomb structural components in IRO. Three relatively mature stereo matching algorithms are selected, namely BM, SGBM, and GC. Table 2 compares and analyzes the algorithms based on a 320×240 size grayscale image.

Table 2: Comparison of three stereo matching algorithms

Stereo matching algorithm	Match Time	Matching effect	Type
BM algorithm	93ms	ordinary	Local matching algorithm
SGBM algorithm	274ms	preferably	Semi global matching algorithm
GC algorithm	>5000ms	preferably	Global matching algorithm

In Table 2, GC has the best matching effect, but its calculation speed is the slowest and difficult to meet the needs of processing honeycomb images. Therefore, the direction is placed on the faster BM and SGBM, and both the two can meet the requirements of image processing. After comparing the detailed results of BM and SGBM, it is found that SGBM has higher matching accuracy and clearer disparity contour map, but its calculation is complex and requires longer calculation time. The two algorithms are applied to the honeycomb perfusion technology, aiming at the iterative reconstruction of honeycomb features and considering the calculation speed and matching effect. The experiment shows that the number of BM binocular stereo matching points meets the requirements of honeycomb corners.

To further verify the feasibility of the stereo matching algorithm, the study compares the BM algorithm with other algorithms for different standard stereo images. By calculating the pixel points of images with different resolutions, the mismatch rate and computational complexity of the comparison algorithm can be obtained. The results are shown in Table 3.

Table 3: Mismatch rate and complexity results of different algorithms

Algorithm	Resolving power				Computational complexity (ms)
	(718×496)	(735×485)	(741×497)	(694×554)	
BM algorithm	0.03	0.16	0.06	0.13	93ms
Directional filter disparity optimization algorithm	6.53	5.82	3.05	2.76	399ms
Stereo matching algorithm for image segmentation	9.47	5.68	6.07	3.15	268ms
Fix window algorithm	3.04	2.83	2.01	1.19	144ms
Adaptive window algorithm	0.65	0.28	0.23	0.18	111ms

From Table 3, the BM algorithm has the lowest false matching rate on stereo images of different standard resolutions, with values of 0.03, 0.16, 0.06, and 0.13, respectively. It also has the lowest value among all algorithms in terms of computational complexity. In addition, the mismatch rate of the adaptive window algorithm is also relatively low, with values of 0.65, 0.28, 0.23, and 0.18, respectively, corresponding to a computational complexity of 111ms. The comprehensive results indicate that the BM algorithm can be used as a binocular stereo matching method for honeycomb perfusion.

Due to the basic parameters of the camera affecting the binocular measurement results, it is necessary to calibrate the camera to establish the connection between the camera ICS and the WCS. The calibration results of the binocular camera are calculated using the Zhang's plane calibration method, and the results are shown in Table 4.

Table 4: Calibration results of binocular cameras

Parameter	Left camera	Right camera
f_x	2348.32330	2348.23270
f_y	2349.00525	2348.88541
u_0	1272.33873	1259.59748
v_0	1025.95665	1017.17410
N	$[-0.00144, -0.00254, 0.00919]$	
G	$[-36.15283, -0.33293, 0.19193]$	

In Table 4, the calibration results of the measurement are obtained from the formula parameters, and then the spatial position relationship between the binocular camera and the calibration board, as well as the projection error analysis of the left and right cameras, are analyzed. The comparative results are shown in Figure 4.

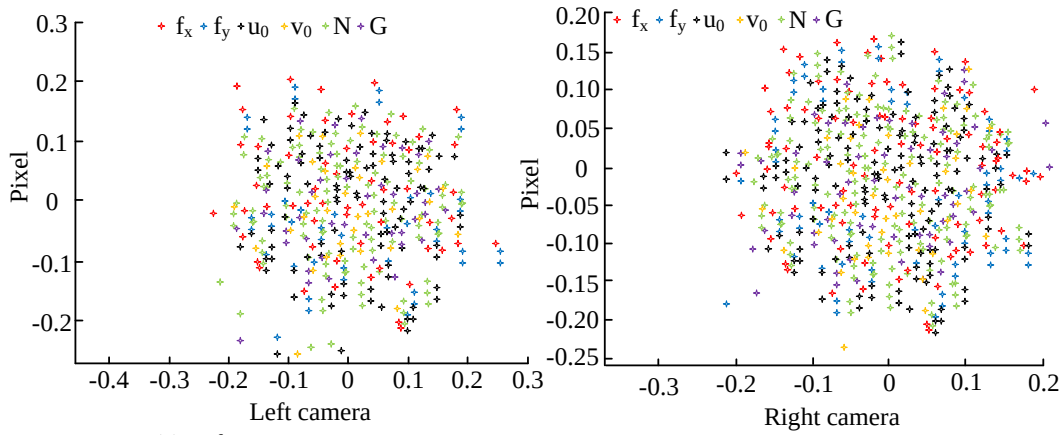

(a) Left camera projection error (b) Right camera projection error

Figure 4: Analysis of camera projection error

In Figure 4, when the parameters of the two cameras are relatively close and converted to a long focal length, the pixel focal lengths of the left camera are 8.10172mm and 8.10407mm. The right camera has a focal length of 8.10140mm and 8.10365mm, which is relatively close to the theoretical focal length of the camera of 8mm. The actual placement distance of the left and right cameras is parallel to the line, and their left and right coordinate system center points are also relatively close to the theoretical midpoint of the camera. The maximum projection error of the left and right cameras is 0.075 pixels, which meets the calibration requirements. 29 honeycomb structural components are selected for positioning measurement and comparison in the experiment, and Figure 5 shows some structural components.

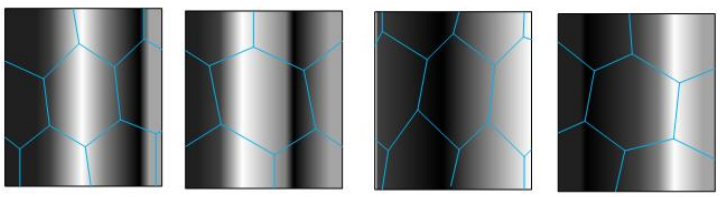

Figure 5: Honeycomb map for partial positioning experiment

From Figure 5, the honeycomb patterns used in the positioning experiment are generally uneven, and there are

numerous honeycomb components, resulting in high feature repeatability. During the measurement and localization process in the target area, IRO is prone to feature point mismatches and localization errors. Therefore, to construct error results, the robot needs to calibrate binocular cameras during the measurement and positioning of perfusion and combine stereo matching algorithms to perform feature matching on the left and right images. Axis lines are established on the six sides of the honeycomb shape. However, as the a-axis is in the same direction as the machine filling head, it is not included. The detailed comparison results are shown in Figure 6.

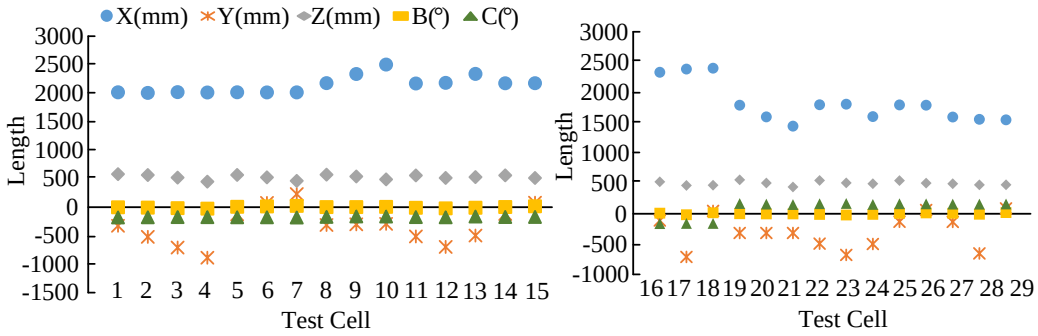

(a) Top 15 cellular positioning results (b) Location results of the last 14 cells

Figure 6: Cellular space positioning results

In Figure 6, the shape, radius, and diameter of 29 honeycomb structural components are inconsistent in length. Factors such as lighting and deformation also affect the error results in the robot coordinate system, so each structural component will not completely coincide. To further evaluate the positioning results, the experiment uses a teaching device to accurately correct the position of the robot to align and test the perfusion position of the honeycomb structural components. Using the precisely calibrated robot position as the target positioning result, Figure 7 is obtained.

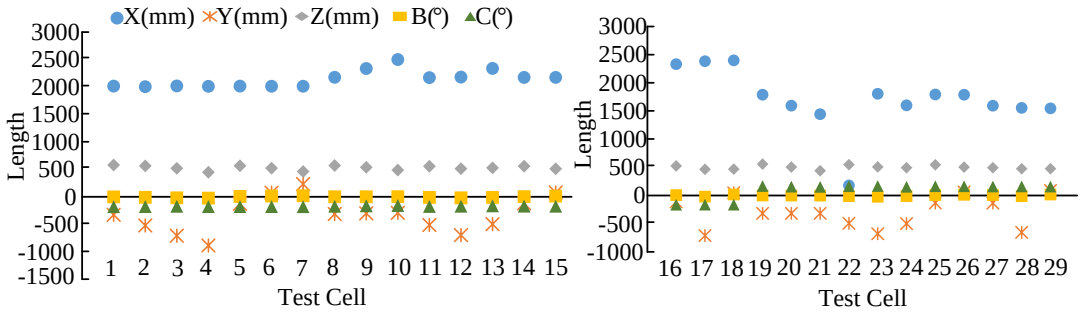

(a) Top 15 Target Positioning Results (b) Positioning results of the last 14 targets

Figure 7: Cellular target location results

In Figure 7, the adjusted target positioning result can efficiently pour the honeycomb parts, thus strengthening the robot positioning function and the efficiency of pouring operation. Afterward, the absolute error between the spatial and target positioning results is calculated using cellular positioning, and Figure 8 is obtained.

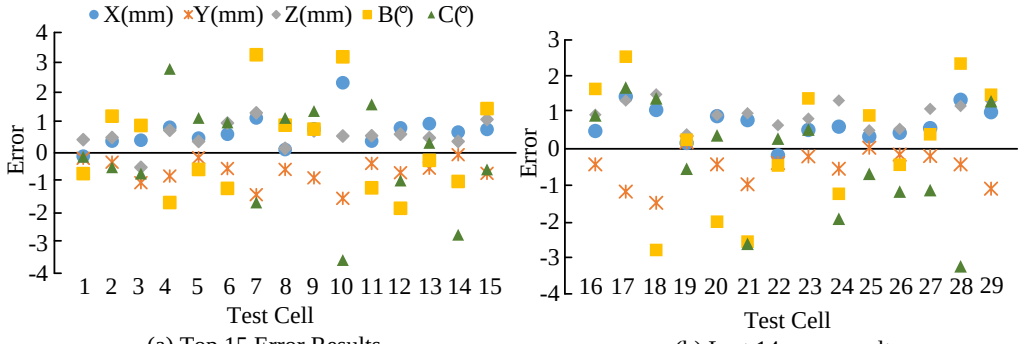

(a) Top 15 Error Results (b) Last 14 error results

Figure 8: Honeycomb positioning measurement error

In Figure 8, the maximum error value on the horizontal axis is 1.16mm, and the mean error value is 0.63mm. The vertical axis is 1.83mm and 0.81mm. The rotation angle is 3.56°, with an average value of 1.37°. Considering the diameter of the robot's infusion head and the diameter of the honeycomb inner cut, it can be concluded that the error is within the allowable range of engineering manufacturing. The positioning accuracy of this cellular positioning method is high. Then the spatial positioning and target positioning results obtained from cellular positioning in the same coordinate graph are displayed, as displayed in Figure 9.

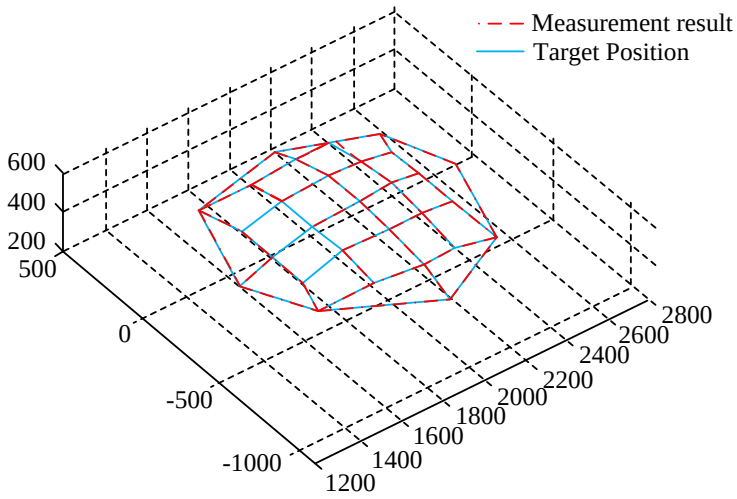

Figure 9: Diagram of measurement results and target location

From Figure 9, the blue color represents the result graph of the target location, and the red part represents the measurement results. The results of the two are generally consistent. Figure 10 shows the error diagram between the two.

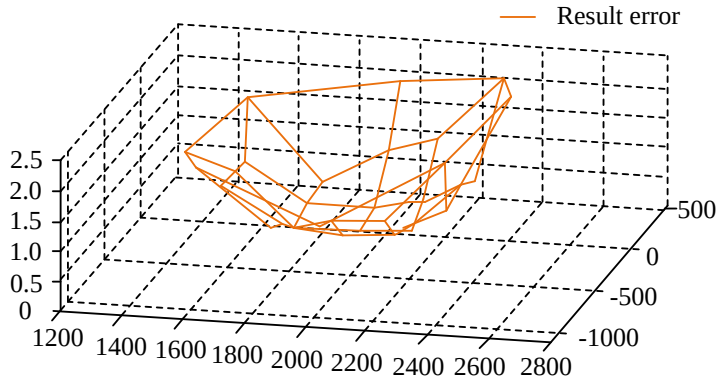

Figure 10: Measurement result error chart

In Figure 10, the measurement error in the central region of the honeycomb structure, defined as the area perpendicular to the surface of the structure and captured by the camera, is markedly smaller than that observed in the surrounding area. The positioning results and target results of the robot's self-defined cellular positioning control software based on MFC can basically maintain errors within 2mm and 4°. It can meet the positioning operation requirements of robot perfusion work later. With the goal of robot precision and intelligent operation engineering, IRO continues to play an important role in industrial automation manufacturing. It also requires corresponding technical references in fields such as medicine and sports to improve the accuracy of robot measurement and positioning.

5 Discussion

In the production of complex and rigorous material structures for IROs, this study utilizes machine vision technology to perform contour recognition, data

measurement, and edge detection on the core components of honeycomb structures. The aim is to enhance the stereo matching and precise infusion of IROs in honeycomb components. According to the matching algorithm of BSV and the measurement results of binocular cameras, it can be concluded that the pixel focal length of the left and right cameras is close to the theoretical focal length of 8mm, indicating the scientific rationality of their camera calibration. In the comparison of stereo matching algorithms, the BM algorithm achieves a matching speed of 93 ms, which is significantly faster than the GC algorithm's >5000 ms, while the latter has better matching accuracy. The trade-off between speed and accuracy highlights the crucial importance of fast decision-making in the practical application of BM algorithm in real-time industry. This is because the local matching type of the BM algorithm can accurately measure the data information of honeycomb components, providing more accurate positions for infusion robots while ensuring operational efficiency. In addition, in the accuracy verification results of IROs for honeycomb components, the error values of the robot for the fifth measurement unit on the axis of the three-dimensional space are 0.22mm, 0.15mm, and 0.1mm, respectively. By integrating the error values of all measurement units, the error results of the infusion operation are within the allowable error range of engineering manufacturing, demonstrating the high accuracy of its positioning method. Compared with Wei H et al.'s binocular vision-guided robotic arm application, although it used line segments and edges as matching units to obtain the mapping relationship between 2D images and 3D scenes, it had good threading application in IRO scenes with a success rate of 70% [9]. The improved image matching algorithm used by Gao G et al. in parallel robot pose detection could significantly reduce the mismatch rate and time consumption, resulting in an average accuracy of 75.66% [15]. The proposed IRO achieves a maximum accuracy of 80% in cellular components, indicating that the binocular vision and stereo matching algorithms used effectively improve accuracy, providing a good technical reference for the practical application of IRO.

6 Conclusion

For the robot measurement and positioning system, a honeycomb perfusion robot positioning technology based on binocular vision algorithm was constructed by combining MFC software control system. Firstly, binocular vision matching algorithms have been studied to improve the measurement results of binocular cameras; Secondly, the binocular solid geometry model was constructed, and the 3D coordinates of the spatial points were calculated using the algorithm. Then, the optimal target matching algorithm was found and applied to both internal and external parameters. The pixel focal lengths of the left camera were 8.10172mm and 8.10407mm, while those of the right camera were 8.10140mm and 8.10365mm. The maximum error value for left and right camera projection was 0.075 pixels. Finally, based on the visual guidance system, the robot positioning and measurement system was constructed. The absolute error between spatial positioning results and target positioning results was obtained using 29 experimental honeycomb structural components. The maximum error value on the horizontal axis was 1.16mm, and the average error value was 0.63mm. The maximum error values on the vertical axis were 1.83mm and 0.81mm. The rotation angle was 3.56°, with an average of 1.37°. Subsequently, based on issues such as the diameter, inner diameter, and angle of the robot's perfusion head, spatial measurements of honeycomb structural components were carried out. By comparing the measurement structures of the target position, the error between the spatial positioning results and the target results was basically within 2mm and 4°, meeting the requirements for robot positioning and perfusion. However, the system lacks practical experimental operation and the application of honeycomb structural components is limited. Therefore, further research and improvement are needed for the development and application of robot positioning measurement technology.

7 Funding statement

The research is supported by Supported by Scientific and Technologial Innovation Programs of Higher Education Institutions in Shanxi, Practical Operation Platform for Simulating Electrical Control System in Intelligent Manufacturing, (No. 2020L0766).

References

[1] Y. Xing and Z. Shao, "Research on robot catching ball based on binocular vision positioning," Academic Journal of Computing & Information Science, vol, 4, no. 6, pp. 72-77, 2021. https://doi.org/10.25236/AJCIS.2021.040612

[2] W. Shao, H. Zhang, Y. Wu, and N. Sheng, "Application of fusion 2D lidar and binocular vision in robot locating obstacles," Journal of Intelligent & Fuzzy Systems, vol. 41, no. 3, pp. 4387-4394, 2021. https://doi.org/10.3233/JIFS-189698

[3] G. Wan, F. Li, W. Zhu, and G. Wang, "High-precision six-degree-of-freedom pose measurement and grasping system for large-size object based on binocular vision," Sensor Review, vol. 40, no. 1, pp. 71-80, 2020. https://doi.org/10.1108/SR-05-2019-0123

[4] J. Zan, "Research on robot path perception and optimization technology based on whale optimization algorithm," Journal of Computational and Cognitive Engineering, vol. 1, no. 4, pp. 201-208, 2022. https://doi.org/10.47852/bonviewJCCE597820205514

[5] J. Zhi, D. Luo, K. Li, Y. Liu, and Q. Liu, "A novel

method of shuttlecock trajectory tracking and prediction for a badminton robot," Robotica, vol. 40, no. 6, pp. 1682-1694, 2022. https://doi.org/10.1017/S0263574721001053

[6] C. Zhang, "Binocular vision navigation method of marine garbage cleaning robot in unknown dynamic scene," Journal of Coastal Research, vol. 103, no. 4, pp. 864-867, 2020. https://doi.org/10.2112/SI103-179.1

[7] H. Ren, "Path avoidance system of intelligent robot based on computer vision. Journal of Physics: Conference Series," IOP Publishing, vol. 2493, no, 1, pp. 012-016, 2023. https://doi.org/10.1088/1742-6596/2493/1/012016

[8] Q. Wang, Z. Meng, and H. Liu, "Review on application of binocular vision technology in field obstacle detection," IOP Conference Series: Materials Science and Engineering, vol. 806, no. 1, pp. 012-025, 2020. https://doi.org/10.1088/1757-899X/806/1/012025

[9] H. Wei and L. Meng, "A stereo matching algorithm for high-precision guidance in a weakly textured industrial robot environment dominated by planar facets," Computer Graphics Forum, vol. 41, no. 1, pp. 288-300, 2022. https://doi.org/10.1111/cgf.14435

[10] J. Zhang, "Target extraction of fruit picking robot vision system," Journal of Physics: Conference Series, vol. 1423, no. 1, pp. 012-061, 2019. https://doi.org/10.1088/1742-6596/1423/1/012061

[11] J. Han, "Study on dynamic target positioning and grabbing based on binocular vision," Academic Journal of Computing & Information Science, vol. 3, no. 1, pp. 78-82, 2020. https://doi.org/10.25236/AJCIS.030108

[12] X. Wen, Y. Hu, B. Yao, Y. Zhao, A. Song, and W. Cui, "Design of dual-arm cooperative leaching robot based on binocular vision," Nanjing Xinxi Gongcheng Daxue Xuebao, vol. 13, no. 3, pp. 304-310, 2021. https://doi.org/10.13878/j.enki.jnuist.2021.03.006

[13] R. Li, R. Wang, and X. Tian, "Binocular vision mechanical arm system based on salient region target recognition," Journal of Physics: Conference Series, vol. 1550, no. 3, pp. 032-059, 2020. https://doi.org/10.1088/1742-6596/1550/3/032059

[14] X. Jian, J. Li, X. Chen, X. Wang, J. Chen, and C. Wu, "A high-precision power line recognition and location method based on structured-light binocular vision," Journal of Advanced Computational Intelligence and Intelligent Informatics, vol. 26, no. 5, pp. 691-697, 2022. https://doi.org/10.20965/jaciii.2022.p0691

[15] G. Gao, Q. Zhang, and S. Zhang, "Pose detection of parallel robot based on improved RANSAC algorithm," Measurement and Control, vol. 52, no. 7-8, pp. 855-868, 2019. https://doi.org/10.1177/0020294019847712

[16] Y. Wang, G. Yang, W. Gao, X. Jia, Z. Huan, and L. Chen, "Rapid detection method of pipe inner diameter based on binocular vision," Journal of Physics: Conference Series, vol. 2402, no. 1, pp. 012-017, 2022. https://doi.org/10.1088/1742-6596/2402/1/012017

[17] J. Zhou, S. Han, Y. Zheng, Z. Wu, W. Liang, and Y. Yang, "Three-dimensional reconstruction of retinal vessels based on binocular vision," Zhongguo Yi Liao Qi Xie Za Zhi Chinese Journal of Medical Instrumentation, vol. 44, no. 1, pp. 13-19, 2020. https://doi.org/10.3969/j.issn.1671-7104.2020.01.003

[18] R. Hu, Y. Xu, Y. Jia, T. Wu, P. Deng, H. Song, and X. Chen, "Power transmission line broken strand repair robot and visual control method," Journal of Physics: Conference Series, vol. 2333, no. 1, pp. 012-019, 2022. https://doi.org/10.1088/1742-6596/2333/1/012019